Exploration of Drug Science

Open Exploration

Open Access Original Article

Study on bioactivities of *Morinda citrifolia* L. fruit hydroalcoholic extracts and detection of novel phytoconstituents by UPLC-Q-exactive orbitrap-tandem mass spectrum analysis

Aslee Tailulu[1], Hanyue Cui[1], Liren Wu[1], Yuhu Shen[2,3], Ping Shi[1,2]*

[1]State Key Laboratory of Bioreactor Engineering, East China University of Science and Technology, Shanghai 200237, China
[2]Laboratory for Research and Utilization of Qinghai Tibet Plateau Germplasm Resources, Academy of Agriculture and Forestry Sciences of Qinghai University (Qinghai Academy of Agriculture and Forestry Sciences), Xining 810016, Qinghai, China
[3]Key Laboratory of Adaptation and Evolution of Plateau Biota, Qinghai Provincial Key Laboratory of Crop Molecular Breeding, Northwest Institute of Plateau Biology, Innovation Academy for Seed Design, Chinese Academy of Sciences, Xining 810008, Qinghai, China

***Correspondence:** Ping Shi, State Key Laboratory of Bioreactor Engineering, East China University of Science and Technology, 130 Meilong Road, Shanghai 200237, China. ship@ecust.edu.cn
Academic Editor: Mozaniel Santana de Oliveira, Federal University of Pará, Brazil
Received: April 20, 2025 **Accepted:** June 18, 2025 **Published:** July 24, 2025

Cite this article: Tailulu A, Cui H, Wu L, Shen Y, Shi P. Study on bioactivities of *Morinda citrifolia* L. fruit hydroalcoholic extracts and detection of novel phytoconstituents by UPLC-Q-exactive orbitrap-tandem mass spectrum analysis. Explor Drug Sci. 2025;3:1008121. https://doi.org/10.37349/eds.2025.1008121

Abstract

Aim: The objective of this study is to ascertain the antimicrobial and anticancer properties of dry *Morinda citrifolia* L. (noni) pulp hydroalcoholic extracts.

Methods: In this study, dry noni samples were immersed in hydro-alcoholic solvents, ethanol (EtOH) and methanol (MeOH). Using the intelligent-flash extractor (KBE-I5) and freeze-vacuum dryer, noni ethanol (NE) and noni methanol (NM) extracts were obtained for antimicrobial testing against bacterial and fungal strains via disc diffusion assay. Cell viability was assessed using the cell counting kit-8 (CCK-8) assay, acridine orange (AO) staining, and western blotting to evaluate anticancer effects on human cancer cells. Novel phytoconstituents were identified using dual-mode ultra-performance liquid chromatography quadrupole exactive orbitrap-tandem mass spectrometer (UPLC-Q-exactive orbitrap-MS/MS) analysis.

Results: Extraction yielded 16.8% for NE and 25.8% for NM. NE minimum inhibitory concentrations (MICs) against *Escherichia coli* (EC), *Saccharomyces cerevisiae* (SC), *Staphylococcus aureus* (SA), and *Streptococcus thermophilus* (ST) being 177, 52, 388, and 283 mg/mL. NM MICs values were 105, 47, 312, and 135 mg/mL, respectively. Anticancer half inhibitory concentrations (IC_{50}s) for NE against human colon adenocarcinoma cell (HT-29) and human bladder cancer cell lines (UMUC-3) were 758 and 899 μg/mL. For NM, IC_{50}s were 1,231 (HT-29) and 1,173 (UMUC-3) μg/mL. Cell death indicators include organelle deformities, AO fluorescence, and autophagy protein expression. In dual ion-scan mode UPLC analysis, 17 distinct phytoconstituents were identified, including 2-Hydroxycinnamic acid, 4-Hydroxycinnamic acid, and riboflavin, known for treating cancer, metabolic dysfunctions, and COVID-19. The 14 constituents were discovered in noni fruit for the first time.

Conclusions: Noni fruit extracts show antimicrobial/anticancer activity and therapeutic potential, establishing noni fruit as a promising food and medicinal source based on composition.

Keywords

Morinda citrifolia L., antimicrobial, anticancer, UPLC-Q-exactive orbitrap-MS/MS, phytoconstituents

Introduction

The *Morinda citrifolia* L., a rubiaceous plant usually referred to as noni, can be found in a number of coastal areas of Asia, South America, Africa, Australia, New Zealand, Hawaii, and the Polynesian Islands [1, 2]. The noni juice is sold in commercial and local markets and is consumed in both formal and informal ways as folk medicine and dietary supplements. The noni fruit-based products are increasingly attracting the interest of consumers [1–3], and they show effective anti-obesity, anticancer, antibacterial, antiviral, and antioxidant [2, 4]. Thus, experts were becoming increasingly interested in the discovery of several phytochemicals which were widely considered to be effective in treating a number of serious health conditions prevalent in humans [2, 5–12]. In order to quickly test, identify, and quantify phytocompounds in the noni fruit extract mixtures, the selection of solvents was crucial [8, 13, 14]. Traditional solvents like ethanol (EtOH) and methanol (MeOH), assisted with evolving extraction methods, were so effective in the extractions of some valuable phytochemicals from the noni plant with the aid of machinery [14–16]. Common extraction techniques include heat reflux extraction, Soxhlet extraction, and maceration because of their low time, energy, or solvent usage. These techniques were frequently employed for the extraction and processing of the noni plant material [17–19]. The phytochemicals from noni were made known by the rapid identification and characterization through chromatography. The gas chromatography-mass spectrometry (GC-MS), capillary zone electrophoresis (CE), headspace-solid phase microextraction/gas chromatography-mass spectrometry (HS-SPME/GC-MS), high performance liquid chromatography mass spectrometry (HPLC-MS), ultra-high performance liquid chromatography coupled to diode array detector and electron spray ionization mass spectrometry (UHPLC-DAD-ESI-MS), high performance liquid chromatography electron spray ionization quadrupole time-of-flight tandem mass spectrometry (HPLC-ESI-QTOF-MS/MS), reverse phase high performance liquid chromatography (RP-HPLC), and ultra-performance liquid chromatography-traveling wave ion mobility quadrupole time-of-flight mass spectrometry (UPLC-TWIMS-QTOF-MS) were among novel techniques for the quantification and identification of these phytocompounds [5, 11, 20–25]. Those techniques are highly effective to swiftly profile phytocompounds in noni due to their validity, sensitivity, and specificity. According to our previous study, the dry noni fruit alcohol extract recovery was achieved with high yield and exhibited effective antimicrobial, anticancer effects, and so on after bioactivity research. Using GC-MS and UPLC, phytocompounds were identified, and so as several were speculated to be novel [18, 19].

In our current study, extracts of the dry noni fruit, NE (noni ethanol) and NM (noni methanol), were obtained using the maceration in an extractor-aided process and later condensed using heat vacuum centrifugation. Test of extracts showed effective antimicrobial and anticancer effects. The 17 phytocompounds were determined via ultra-performance liquid chromatography quadrupole exactive orbitrap-tandem mass spectrometer (UPLC-Q-exactive orbitrap-MS/MS). According to the Human Metabolome Database (HMDB), Food Database (FOODB), and literature review, 3 compounds were confirmed to have been used in the treatment of health-related dysfunction. The 14 unused compounds were speculated to be novel. This study will enrich the knowledge and improve the noni fruit for health and food purposes in the future.

Materials and methods

Plant material

Noni fruits collected in June 2019 from Wuzhishan, Hainan, China, had their pulps harvested at stage 5 (25 days pre-ripening). The fruits were processed and dried, stored in 161 g containers (Lot GH/T 1091, SCI10646900100011) for use in the study [1, 2, 18, 19]. See Figure 1A and B.

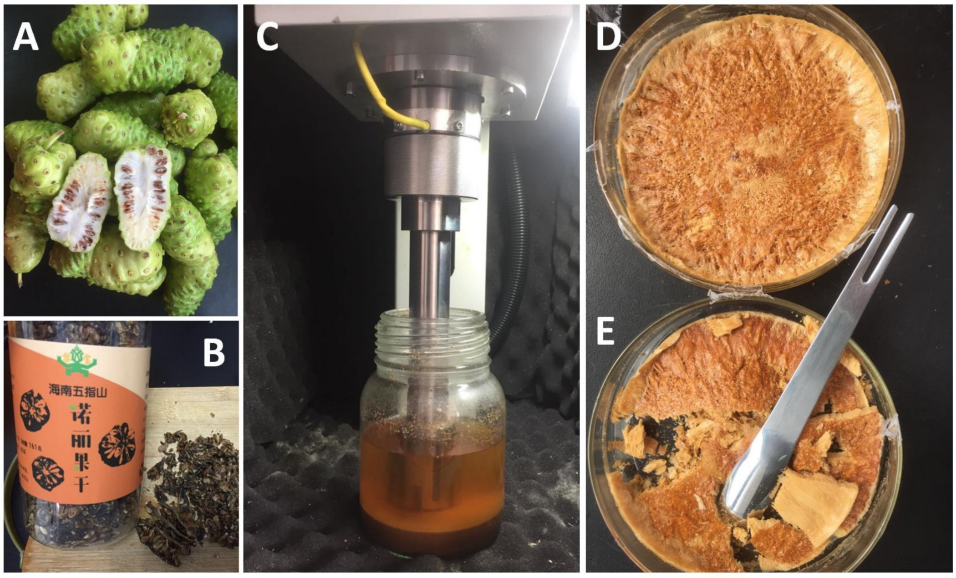

Figure 1. The various stages of noni fruit processing are illustrated, which include the procurement of fresh pulp to powdered extracts. (**A**) The harvest of fresh noni pulp, which was harvested and purchased from Wuzhishan, Hainan, at stage 5 (25 days pre-ripening) [1, 2, 18, 19]. (**B**) The dried, processed, and stored noni fruit slices are semi-crushed into manageable pieces, a crucial step for further processing. (**C**) The crushed samples are then soaked and macerated intro hydro solvent solution. The sample is pulverized by the KBE-I5 extractor into noni grounds. The final dried products were processed into dried powder using vacuum freeze-drying for 24 h, resulting in (**D**) NE and (**E**) NM. NE: noni ethanol; NM: noni methanol

Reagents

The extraction solvents, EtOH, ≥ 99.5% and MeOH, ≥ 99.5% were obtained from Sigma—Aldrich in Shanghai, China. Acetonitrile (AcN, ≥ 99.5%) was procured from Titan Scientific, also based in Shanghai, China. Formic acid (FA, ≥ 99%) and MeOH used for UPLC analysis were purchased from Merk, Shanghai, China. All the reagents used were of standard chromatography grade. The distilled water utilized in the process was treated using a Milli-Q system (Millipore Elix 3, Millipore, Shanghai, China), ensuring high purity [18, 19, 21–24].

Microbial strains and cell lines

The fungal strain of SC (*Saccharomyces cerevisiae*) and bacterial strains of EC (*Escherichia coli*), SA (*Staphylococcus aureus*), and ST (*Streptococcus thermophilus*) were obtained from the China Industrial Microbial Species Preservation and Management Centre in Shanghai, China. The EC, SA, and ST strains were cultured in Luria-Bertani (LB) medium, while the SC strain was cultured in yeast peptone dextrose (YPD) medium at 30°–37°C in a microbial incubator (Jinghong Equipment Co., Ltd, China). The LB medium was composed of 0.5% yeast extract, 1% peptone, and 1% sodium chloride (NaCl) (w/v), as per standard protocols. The YPD medium contained 1% yeast extract, 2% peptone, and 2% glucose (w/v). To prepare solid medium, 1.5% (w/v) agar was added to each medium, dissolved in distilled water, and then sterilized using an autoclave (Heng Technology Co., Ltd, China) [26–29]. The HT-29 (human colon adenocarcinoma cell), UMUC-3 (human bladder cancer cell), human umbilical vein endothelial cell (HUVEC), and normal human uroepithelium bladder cell line (SVHUC-1) were procured from the Institute of Cell Biology (Shanghai, China). The identity of the cell lines was confirmed through STR (Short Tandem Repeat) analysis and consistent with their known identities in databases of American type culture collection (ATCC), and International cell line authentication committee (ICLAC) for verification in our past studies (data are not shown) [18, 19, 30–36]. Cell lines were maintained in Dulbecco's modified Eagle's medium (DMEM) and Ham's F-12K medium (mixture of DMEM and F-12) sourced from Gibco/Invitrogen, Camarillo, CA, USA. Additionally, Roswell Park Memorial Institute (RPMI) 1640 Medium was utilized, provided by Gibco, ThermoFisher, Shanghai, China. Each culture mediums were supplemented with 10% fetal bovine serum (FBS), obtained from PAN Biotech, Aidenbach, Germany, along with 1% antibiotics consisting of 10,000 U/mL penicillin and 10 mg/mL streptomycin from Solarbio Life Science, Beijing, China. The cells were incubated at a temperature of 37°C and a carbon dioxide (CO_2) concentration of 5% within a cell incubator [18, 19, 30–36].

Preparation and extraction method of noni extract

The noni extracts were obtained through a process involving dissolvable maceration with a 1:4 ratio of water to solvent, aided by the KBE-I5 extractor processor (Shanghai Kunbo automation equipment Co., Ltd). See Figure 1C. Initially, 40 g of dry noni fruit grounds were soaked in 500 mL of hydroalcoholic solvents, either EtOH or MeOH, and preserved at 4°C for 120 h. The samples were then pulverized using the KBE-I5-extractor at a rotation speed of 1,000 rpm in dual cycle mode, with a rate of 1 min per cycle for 3 min. Following this, the sample was then centrifuged for 7 min at 3,000 rpm, removing precipitants. The supernatants were then filtered through a 0.45 µm organic filter twice to ensure purity. The filtered supernatants were poured into petri dishes and placed in a –80°C freezer for 48 h to freeze the samples. Subsequently, the frozen samples were subjected to freeze-drying using a vacuum-sealed chamber dryer equipped with a pump and refrigerator vapor trap system at –55°C for 24 h to concentrate the extracts. The equipment used for the extraction and concentration processes was from reputable manufacturers, including Shanghai Kunbo Automation Equipment Co., Ltd, for the KBE-I5 extractor processor and Thermo Scientific, USA, for the freeze dryer. The dry powder extracts, seen in Figure 1D and E, were stored in a sealed desiccator, protected from light, for future use. Prior to UPLC analysis, samples of both extracts were preconcentrated, filtered twice, and degassed using sonication. To optimize the auto-running sequence and achieve reliable results, multiple trial runs were conducted. All experimental data were recorded in triplicate to ensure accuracy and reliability. Stock samples (4 mL) were prepared from each extract at a concentration of 2 g/mL with 0.01% dimethyl sulfoxide (DMSO). Specifically, 8 g of each extract powder was dissolved in a mixture of DMSO and water at a ratio of 0.1:1,000 (v/v) [13, 14, 17–19].

Zone inhibition assay for antimicrobial effect

The agar plate disc diffusion assay was conducted to assess the antibacterial activity, following the guidelines established by the Institute of Clinical and Laboratory Standards (CLSI) and the European Committee on Antimicrobial Susceptibility Testing (EUCAST) [18, 19, 37–39]. The EC, SA, and ST strains were first pre-incubated in 10 mL of LB, and the SC was pre-incubated in YPD liquid medium at 30°–37°C overnight. Sterilized agar culture medium (20 mL) was prepared and solidified onto petri dishes. A 200 µL aliquot of the individual strains' standard inoculum was daubed onto the agar surface. The extract stock samples were serially diluted to the assigned test concentrations before being used in each test. A 30 µL aliquot of each pre-diluted extract sample was applied to filter paper discs placed on top of the inoculum agar surface, and the samples were then incubated overnight for 24 h. Kanamycin sulfate (χ = 10 mg/mL) was used as a positive control for the selected test strains. The MIC (minimum inhibitory concentration) of each extract was determined by measuring the inhibition zones [18, 19, 21, 26–29].

Cell viability, organelle, and autophagy morphology assay for anticancer effect

A total of 3×10^4 cells of SVHUC-1 and HUVEC cell lines and 2×10^4 cells of UMUC-3 and HT-29 were cultured in triplicate using 96-well plates at 37°C in 5% CO_2 level. The cells were incubated until they reached 80% confluence, and then the test groups were treated with NE and NM extracts at concentrations between 200 and 1,500 µg/mL (w/v). A 0.1% DMSO sample was used as a control. After 72 h, cell viability was assessed using the CCK-8 (cell counting kit-8) assay, 10 µL per well of reagent in accordance with the manufacturer's instructions (Dojindo, Tokyo, Japan). The absorbance was read at 450 nm with a Genios multimode reader (Tecan GENios Pro, Tecan Group Ltd, Mannedorf, Switzerland). The IC_{50} (half inhibitory concentration) was calculated using GraphPad Prism, indicating the toxicity of the extracts [30]. For the study on the morphology of HT-29 and UMUC-3 cell lines, the cells were cultured in a 24-well plate at a density of 8×10^6 cells/well. Each group of extract samples was treated with its respective IC_{50} values. After 72 h of treatment with NE and NM, the HT-29 and UMUC-3 cell samples, along with the control group, were rinsed three times using phosphate-buffered saline (PBS). The samples were resuspended in 1 mL of PBS and observed under white light using a Nikon A1R confocal laser scanning microscope, with an excitation wavelength of 488 nm and emission wavelength: 510–540 nm [18, 30, 34–36, 40–42].

Fluorescence staining with AO (acridine orange) stain (Sigma Aldrich, USA) was utilized to examine cell autophagy in HT-29 and UMUC-3 cell lines. The lysosomotropic dye AO emits a green/yellow to orange/red fluorescence in a pH-dependent manner, as it protonates to form aggregates that emit bright red fluorescence at low pH [40]. The cells were cultured in a 24-well plate at a density of 8×10^6 to 12×10^6 cells/well and treated with the respective IC_{50} values of each test group for the NE and NM extract samples in triplicate. Following a 72 h treatment, the cancer cells were washed three times with PBS and then stained with 1 mL AO (1 µg/mL AO in PBS) for 30 min at 37°C in the dark. The samples were subsequently observed using a Nikon A1R confocal laser scanning microscope with an excitation wavelength of 488 nm and an emission wavelength of 510–540 nm at a scale of 20 µm [41].

Western blotting

The HT-29 and UMUC-3 cell lines were cultured in 6-well plates at a density of 120×10^6 cells/well. These cells were then treated with the respective IC_{50} values determined for each test group, specifically for NE and NM application, with all samples processed in triplicate. Following treatment, cell lysis and protein extraction, an essential step for subsequent western blotting analysis, were performed as previously described [33, 34, 40–42]. Following treatment with NE and NM extract compounds, the cell lines were subject to lysis using 200 mL lysis buffer that contains 1.19 g of 4-(2-hydroxyethyl)-1-piperazineethanesulfonic acid (HEPES), 0.028 g magnesium chloride ($MgCl_2$), 50 mM tris (hydro methyl)-aminomethane buffer (Tris/pH 7.4), 100 mM NaCl, 5 mM disodium salt dyhydrate (Na/EDTA), 0.1% sodium dodecyl sulfate (SDS), 1% Triton X-100 and 2% glycerol. Supplements to the lysis buffer include: 0.1 M phenylmethylsulphonyl (PMSF) 1 µL, 1 M dithiothreitol (DTT) 10 µL, 1 M sodium 3-glycerophosphate (β-GP) 20 µL, 1 mM sodium vanadate (Na_3VO_4), and 10 µL protein inhibitor for every 1 mL of the lysis buffer. The protein concentration was determined using the Bradford assay with BSA as a standard. 50 µg protein extracted from the lysates was separated on 12% SDS-PAGE (polyacrylamide gel electrophoresis). After they were separated, they were transferred to polyvinylidene fluoride (PVDF) membranes (Buckinghamshire, UK) [24, 30, 33–36, 40, 41, 43]. The target proteins were blocked with 5% skimmed milk and then blotted with specific primary antibodies as follows: Beta Actin antibody (β-Actin, ab8227, Abcam, UK), and rabbit polyclonal antibody (LC3A I/II, 4599, Cell Signaling Technology, USA). Subsequently, the membrane was washed three times with tris-buffered saline-Tween 20 (TBST) solution and incubated with goat anti-rabbit IgG horseradish peroxidase (HRP)-coupled secondary antibodies (111-036-003, Jackson Immuno Research Laboratories, USA). The enhanced chemiluminescent (ECL) protein imprint detection kit (Tian Gen Biotech, Shanghai, China) was used to detect the immunoreactive proteins, and the signal density was measured using the Tanon 6200 (Tanon Science & Technology Co., Ltd, Shanghai, China) [33–36, 39, 40].

UPLC instrumentation assessment

The UPLC-Q-exactive orbitrap-MS/MS analysis was conducted using a Nexera UPLC system. The system is equipped with a column oven, sample management with a flow-through needle, binary solvent management, a UV spectroscopy detector, and two individual distribution pumps (Shimadzu Corporation, Japan). A Fourier transform ion cyclotron resonance mass spectrometer (FTMS) with magnetic mass spectroscopy and an electrostatic field mass spectrometer, both supported by an electrospray ionization (ESI) source, is located in the Q-exactive orbitrap. The fragmentation data-dependent spectra were scanned using a low collision-induced dissociation (LCID) and a high collision-induced dissociation (HCID) energy source, as well as ESI sources, all of which were supplied by ThermoFisher Scientific, USA. The mixture was fractionated on a Waters Acquity UPLC HSS-T3 end-capped column (100 mm × 2.1 mm, 1.8 µm, Waters, Ireland). The temperature of both the column and the sample was maintained at 45°C. To optimize the auto-run procedures and results, a 0.1 mg/mL (w/v) extract sample from each NE and NM extract was diluted with MeOH, filtered, degassed, and then used for the analytical tests. An injection volume of 3 µL was injected into the system mobile phase flow rate set at 0.35 mL/min. Eluate analysis was monitored at 365 nm UV within a range of 200–400 nm [18, 19, 21–24]. The two mobile phases were filtered through a

0.22 µm organic filter and degassed by sonication for 1 h prior to use. The linear elution gradient was configured as follows: an initial hold at 5% B from 0.01 to 2 min, 5% B (2–2.5 min), followed by another 5% B from 2 to 2.5 min, then a linear increase to 15% B from 2.5 to 7 min, further increase to 55% B from 7 to 9.5 min, then to 90% B from 9.5 to 12 min, held at 90% B from 12 to 13 min, and finally 5% B from 13–14 min. The instrument control, data processing, and recording were performed using Xcalibur® data software (Version 4.2.47, ThermoFisher Scientific, USA) [18, 23, 24]. In both positive (ESI+) and negative (ESI–) settings, the ionic fragments that controlled the UPLC system remained stable, showing increased intensity and a well-defined peak. Consequently, ESI was utilized for continuum data acquisition with a scan time of 0.2 sec over a mass-to-charge range of 50–1,000 m/z in both ESI+ and ESI– modes. To assess the mass mode, dual mass acquisition mode scan functions were employed. Specifically, in the trap cell, the LCID scan was set to a collision voltage of 10 V, whereas in the transfer cell, the HCID scan was configured with a collision voltage ranging between 20 and 60 V. The mass spectra acquired during the full range acquisition encompass ESI source parameters and ion scanning at a normalized HCID collision energy for fragmentation, which is dependent on a data-dependent scan mode. Nitrogen gas was used as both the collision gas and the source of ionization. Additional parameters used include a desolvation gas temperature of 550°C, a source temperature of 120°C, and a capillary voltage of 1.5 V; others, such as gas flow, auxiliary gas flow rate, capillary temperature, and cone voltage. The auxiliary gas flow rate is set at 10 arbitrary (Arb) units for both ESI+ and ESI– modes. The capillary temperature is maintained at 320°C; the cone voltage is set to 3.8 kV. The full scan resolution is 70,000 m/z, and the HCD-MS/MS (high energy collision C-trap dissociation tandem mass spectrometer) resolution is 17,500 m/z, with a mass scan range between 100 to 1,200 m/z. The sheath gas flow rates are 40 and 35 Arb units for ESI+ and ESI– modes, respectively, and the spray voltage is set at 3.5 kV for ESI– and –3.0 kV for ESI– [18, 19, 21–24].

Analysis of raw data and phytoconstituents verification

Xcalibur was used to acquire raw data from the analyses conducted in full-scan mode. The Metabolomics Innovation Center (TMIC) provided quantitative metabolomics services for biomarker discovery and validation kits, utilizing a chemical reference library of standards generated from the HMDB (Version 5.0) and FOODB (Version 1.0). This library assists in the identification of confirmed compounds. Peak selection, adduct deconvolution, and feature annotation were employed to process the data. For metabolite annotation, a tolerance of 5 ppm was applied to both precursors and fragment mass, and an isotopic similarity threshold of over 60% relative to the HMDB was used to verify metabolite identities. Additionally, the cosine similarity algorithm integrated into Mass Bank was utilized to compare the calculated tandem MS/MS fragmentation spectra with corresponding reference spectra. This cosine similarity method assigns fragmentation scores, ranging from 0% (indicating a poor match) to 100% (indicating an excellent match), based on how closely the evaluated MS/MS spectrum aligns with the reference spectra. Due to non-matching or missing peaks in the evaluated tandem mass spectrum compared to the referenced spectrum, the overall score-which was initially 30, can vary between 60% in a worst-case scenario and 100% in the best-case scenario. To evaluate both the overall score and metabolite identification, five different properties are considered for each feature: isotope distribution, mass, retention time (RT, t_r = min), collisional cross section (CCS) value, and fragmentation score [18, 19, 21–24]. Each of these individual scores ranges from 0 to 100, where any property that does not match the reference data is assigned a score of 0. The overall score is then calculated as the mean of these five values. When discrepancies such as missing or non-matching peaks are observed between the evaluated dual mass spectrum and its reference, adjustments to the overall score occur. For instance, although an initial overall score 30% might have been recorded, these discrepancies can result in a score of 60% under the worst-case scenario or even 100% under optimal conditions. To assess both the overall score and the accuracy of metabolite identification, each feature is evaluated using 5 key properties: isotope distribution, mass accuracy (mass quantity), RT, CCS value, and fragmentation score. Each property is scored on a 0 to 100 scale, with a score of 0 being assigned if a property does not match the corresponding reference data. The final overall score is calculated as the mean of these five individual scores, and the compounds are

ultimately selected based on this comprehensive scoring process combined with fragmentation analysis. The identity of each confirmed compound was determined to be more reliable with higher scores and fragmentation scores when searching the MS/MS spectrum against the HMDB, a comprehensive library that includes metabolites from various mixtures with referenced LC-MS/MS data and predicted nuclear magnetic resonance (NMR) spectra. This library offers precise predictions of mass, retention indices, and collision cross-section data, thereby enhancing compound identification [18]. The hyperlinked databases of HMDB, FOODB, the Small Molecule Pathway Database (SMPDB), Drug Bank, and the Toxin and Toxin Target Database (T3DB) provide valuable support for the efficiency and reliability of phytocompound identification [23, 24, 44]. The dataset comprised a comprehensive array of information on compound identification, including each compound's ID, adducts, molecular formula, score, fragmentation score, mass error (within 5 ppm), isotope similarity (greater than 60%), theoretical isotope distribution, a web link directing users to the HMDB and FOODB, a detailed compound description, RT (min), and m/z values. For each individual compound, those numbered in order of elution RT were selected based on their high fragmentation scores, as well as their overall scores and isotopic similarity scores. Furthermore, the mass ratio (m/z) detected in the database was evaluated in Excel data format, and the mass error was assessed to be within 5 ppm [18].

Statistical analysis

All values were given as a mean ± SD, and the data analyses were conducted using GraphPad Prism software (version 8.2.0) with the Microsoft Excel 2017 data analysis add-in. A Student's *t*-test with a significance level of $^{***}P < 0.001$ was used to identify statistically significant differences between the test groups and the control group. The experiments were repeated three times, and the data were presented as the mean ± SD (for each group, $n = 3$). The chemical structures of the phytocompounds were drawn using the ChemDraw software (Revvity Signals Software, Inc., 2023).

Results

Noni fruit hydroalcoholic extracts

The net weight of the NE extract was 6.72 g in Figure 1D, while that of the NM extract was 10.30 g, as seen in Figure 1E. These values were obtained after processing. The extrapolated recovery rates for both extracts were 16.8% for NE and 25.8% for NM, respectively.

Antimicrobial effect of extracts on strains

The antibacterial efficacy of the substance was evidenced by the formation of a clearly discernible inhibition zone in the disk diffusion assay [18, 19]. Seen in Figure 2, the NE extract versus A: EC, B: SC, C: SA, and D: ST. For the extract NM against strains in E: EC, F: SC, G: SA, and H: ST. The inhibition zone diameters (mm) were assessed, and the MIC values of each extract on the tested strains were also estimated. For the NE extract, inhibition zone diameters (mm) corresponding to the MIC values were recorded as follows: EC (10.06 ± 0.08), SC (11.15 ± 0.21), SA (10.09 ± 0.14), and ST (10.05 ± 0.09). For the NM extract, the inhibition zones were as follows: EC (11.75 ± 0.07), SC (10.63 ± 0.15), SA (9.84 ± 0.17), and ST (9.65 ± 0.10). The MIC value of the NE extract against EC strain is 177 mg/mL, SC 52 mg/mL, SA 388 mg/mL, and ST 283 mg/mL. The MIC of the NM extract against EC strain is 105 mg/mL, SC 47 mg/mL, SA 312 mg/mL, and ST 135 mg/mL, respectively.

Anticancer effect of extracts on cells

Using the CCK-8, the cytotoxicity of NE and NM extracts on HT-29, UMUC-3, HUVEC, and SVHUC-1 cell lines was evaluated. The data showed that both extracts reduced the viability in Figure 3, A: HT-29 and C: UMUC-3 cells after a 72 h test period. The cell growth of B: HUVEC and D: SVHUC-1 was exponentially normal after the test, similar to NE and NM extracts. The IC_{50} extrapolated for each extract showed NE with a value at 758 µg/mL and NM valued at 1,231 µg/mL against HT-29. The NE value at 899 µg/mL and the NM value at 1,173 µg/mL against UMUC-3. Additionally, microscopic observations of cell organelles morphology after

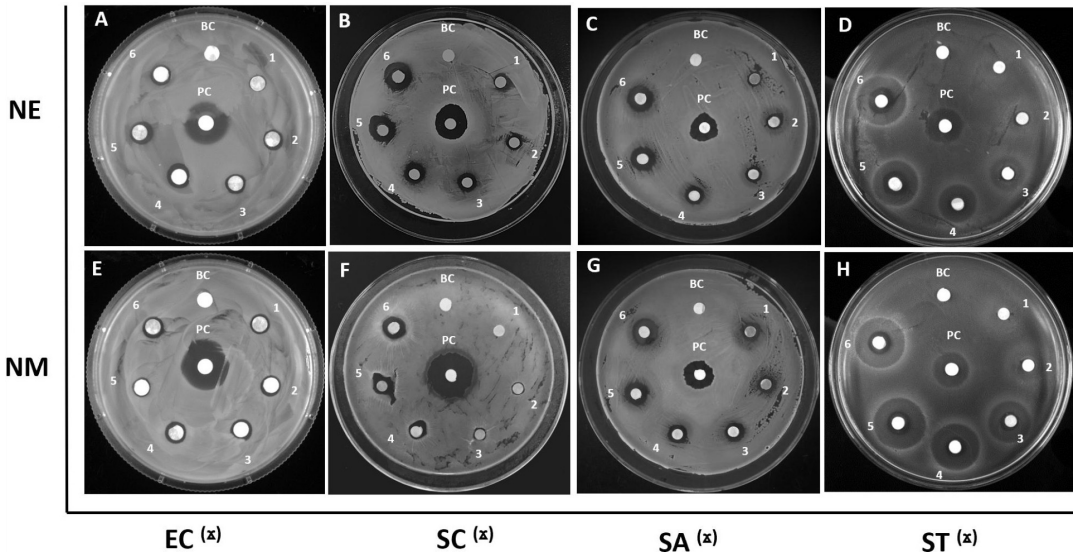

Figure 2. The inhibition zones demonstrate the antibacterial effect of NE and NM extracts on the EC, SC, SA, and ST strains. The concentrations of NE and NM extracts ranged from 900 mg/mL to 5,000 mg/mL, corresponding to positions 1 through 6 in a clockwise direction. Figure panels (**A)** to (**D)** illustrate the antimicrobial effect of NE extract against EC, SC, SA, and ST strains, respectively. The antimicrobial effects of the NM extract are shown in Figure panels (**E)** to (**H)** for EC, SC, SA, and ST strains. BCs using a 10% solution of extract solvents EtOH and MeOH were included. A PC consisting of 10 mM KanS (ɤ) was used for comparison with the assigned strains accordingly. BCs: blank controls; EC: *Escherichia coli*; EtOH: ethanol; KanS: kanamycin sulfate; MeOH: methanol; NE: noni ethanol; NM: noni methanol; PC: positive control; SA: *Staphylococcus aureus*; SC: *Saccharomyces cerevisiae*; ST: *Streptococcus thermophilus*

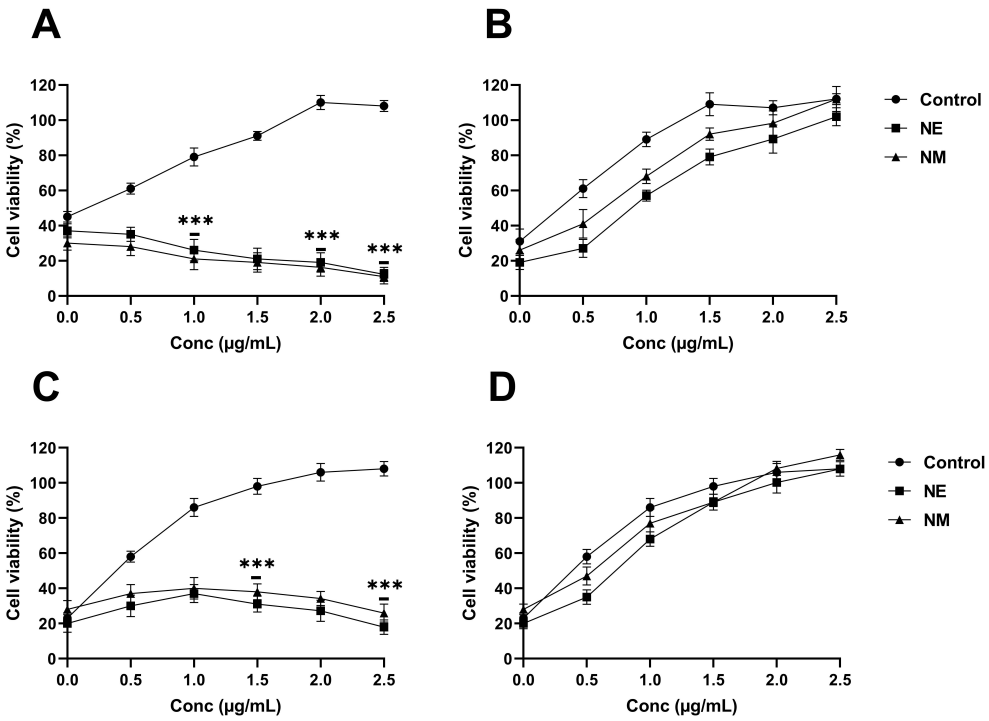

Figure 3. Cell viability of both normal (HUVEC and SVHUC-1) and cancer cells (HT-29 and UMUC-3), after being treated with extracts for 72 h. All cell lines were incubated with 0.1% DMSO (control) or with NE and NM extracts at concentrations between 200 and 1,500 µg/mL (w/v) prior to the cell viability test. Student's *t*-test data analysis expressed statistically significant difference values of ****P* < 0.001 of all treated groups versus the respective control groups as marked on graphs. (**A**) HT-29, (****P* < 0.001 for both NE/NM extracts at concentrations 1.0, 2.0, and 2.5 µg/mL versus control group), (**B**) HUVEC, (**C**) for UMUC-3 (****P* < 0.001 for both NE/NM extracts at concentrations 1.5 and 2.5 µg/mL versus control group), and (**D**) SVHUC-1. DMSO: dimethyl sulfoxide; NE: noni ethanol; NM: noni methanol

IC_{50} treatment groups of each extract after 72 h under white light showed deformed and irregular-shaped cellular structures in HT-29 and UMUC-3. Seen in Figure 4 are the control groups of A to D, and the treated groups are E to H.

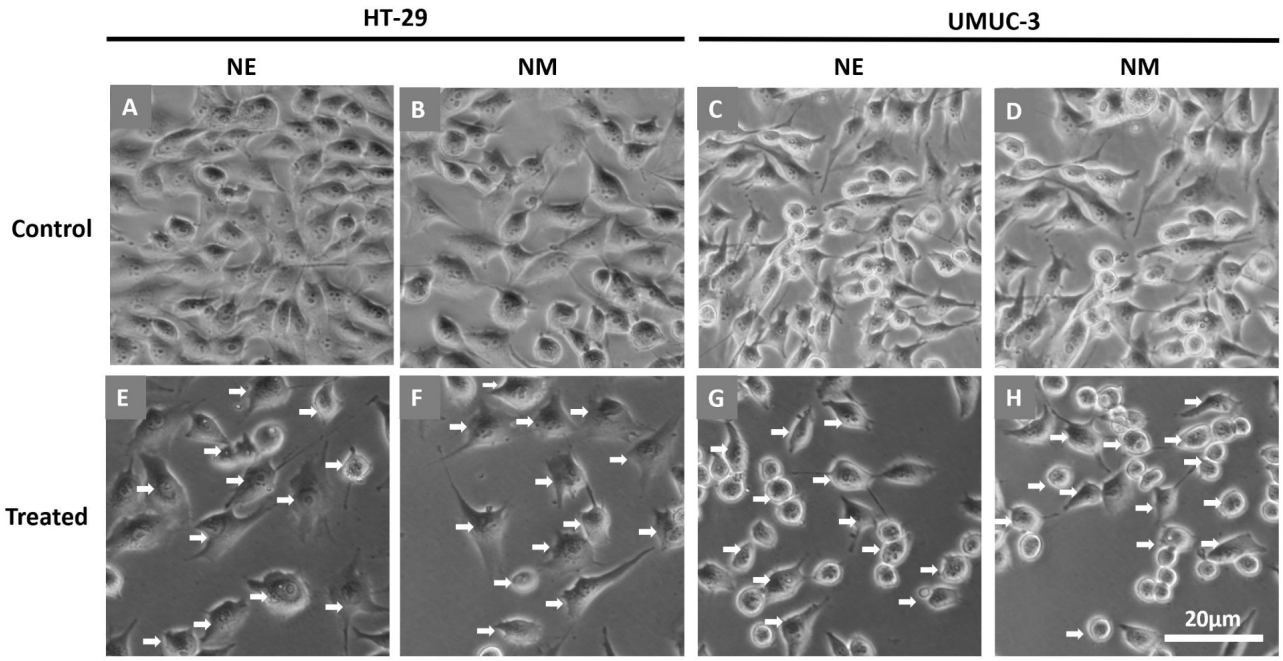

Figure 4. Illustrates the cell morphology of cancer cell lines after treatment with IC_{50}s of NE and NM extracts for 72 h. The control groups, (**A**) and (**B**) for HT-29 and (**C**) and (**D**) for UMUC-3, served as references. The treated groups, (**E**) and (**F**), were exposed to NE and NM extracts on HT-29 cells, respectively, while (**G**) and (**H**) were treated with NE and NM extracts on UMUC-3 cells. The scale bar, representing 20 µm, is indicated at the bottom right corner. The arrows highlight the deformed, shriveled, and ruptured cell membranes of the HT-29 and UMUC-3 cell lines after treatment, which is consistent with the morphological changes observed in apoptotic cells. IC_{50}: half inhibitory concentration; NE: noni ethanol; NM: noni methanol

Autophagy induced by extracts on HT-29 and UMUC-3 cells

The AO fluorescent staining was used to investigate the effect of NE and NM extracts on HT-29 and UMUC-3 cells, in which the test group with extract was investigated for the induce and accumulation of autophagy vesicles observed under the cancer cell lines by the florescence emission in Figure 5. As a result of cell death, based on the decrease of cell viability there autophagic bodies were observed among the treated group seen in Figure 5E and F, inflicted by compounds NE and NM compared to the control groups Figure 5A and B for the HT-29 cell. There were also autophagic bodies were also observed in the treated group in Figure 5G and H by extract NE and NM in comparison to the control groups, Figure 5C and D for the UMUC-3. In addition, the effect of the extract NE and NM on autophagy-related proteins in HT-29 and UMUC-3 cells was then examined using western blot in Figure 6A. The ratio of LC3A II/I in cells treated with both extracts individually was clearly expressed and evaluated in relation to those in their control groups, see Figure 6B.

Phytoconstituents analysis in NE and NM identified by UPLC-Q-exactive orbitrap-MS/MS

Both NE and NM extract chromatogram results showed the presence of compounds by several peak counts at RT against relative abundance, and both in selective ion polarized mode scans, according to the selective ions and elution order obtained from the UPLC-Q-exactive orbitrap-MS/MS analysis graphs seen in Figures 7 and 8. A mass spectrometer with dual mass-to-charge ratio scan, a primary mass score range (max 60%), and a secondary fragmentation maximum score (max 100%) was acquired to identify all compounds. As seen in Figure 7A (top ESI–) and Figure 7B (bottom ESI+), base peak intensity (BPI) graphs showed migration time and abundance relative intensity (AUD) of individual compound peaks. NE extract showed 10 peaks, and they were identified by searching the chemical reference library of standards from the FOODB and HMDB databases, as listed in Table 1. The HMDB database hyperlinks databases of the SMPDB, Drug Bank, the T3DB, and the FOODB, aiding efficiency and reliability in identifying each compound [44, 45].

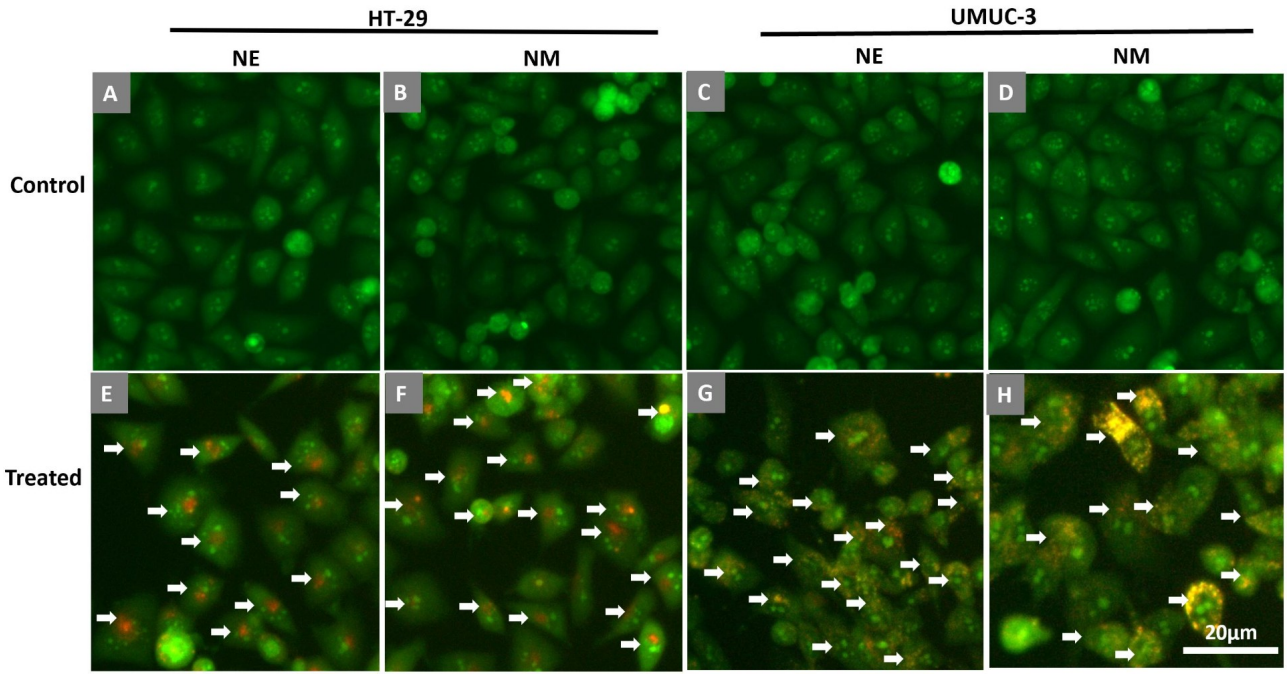

Figure 5. Illustrates the effects of NE and NM on the intercellular morphology of HT-29 and UMUC-3 cells. The control group panels (**A)** to (**D)** and the NE- and NM- treated groups (**E)** to (**H**) of HT-29 and UMUC-3 cell lines display autophagic vacuoles after AO staining when observed under fluorescence microscopy. The arrows indicate the staining of HT-29 and UMUC-3 cell lines with AO after treatment, which is consistent with the presence of autophagy vacuoles, suggesting autophagy as a cell death pathway within the treated cells. AO: acridine orange; NE: noni ethanol; NM: noni methanol

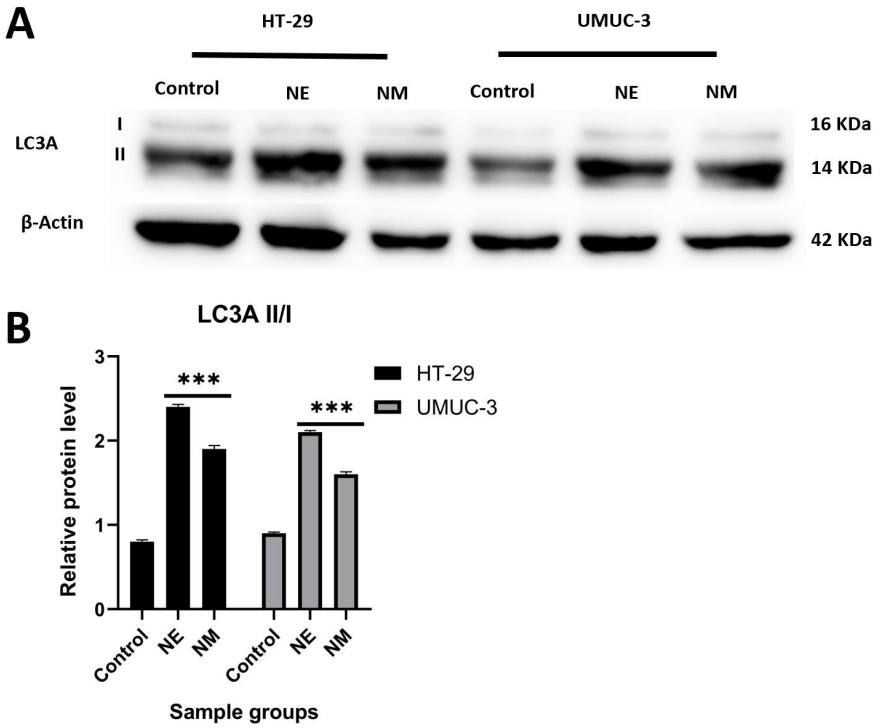

Figure 6. Western blot analysis to investigate the effects of NE and NM extracts on the expression of autophagy-related proteins in HT-29 and UMUC-3 cell lines after a 72 h treatment period. (**A**) The visual expression of LC3A I/II, a protein relevant to autophagy, was examined after being treated with NE and NM extracts. (**B**) The relative protein levels of LC3A II/I expression were assessed in HT-29 and UMUC-3 cells after treatment. The analysis utilized an independent samples Student's *t*-test to compare protein levels, with a significance level of ***$P < 0.001$. Statistically significant differences in protein levels were observed between HT-29 and UMUC-3 cells treated with NE and NM compared to their respective control groups. The experiments were repeated three times, and the data were presented as the mean ± SD (for each group, $n = 3$). NE: noni ethanol; NM: noni methanol

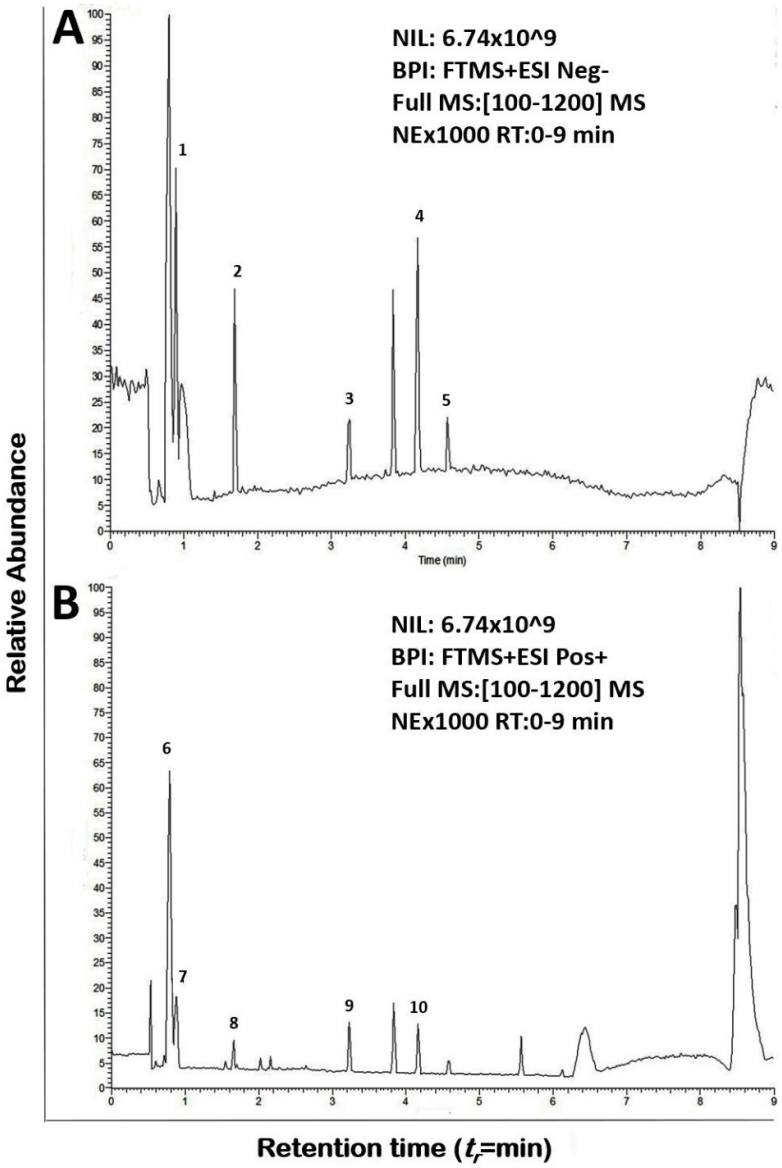

Figure 7. Illustration of the UPLC analysis chromatogram, which displays the peak counts and retention time (*tr* = min) relative to the abundance of both negative (ESI–) and positive (ESI+) ions BPI graphs (NE extract). The chromatograms are divided into two sections: (**A**) showing the peak counts of identified compounds peaks (1–5) in the NE extract using ESI–, (**B**) displaying the peak counts (6–10) in the NE extract using ESI+. BPI: base peak intensity; ESI: electrospray ionization; NE: noni ethanol; UPLC: ultra-performance liquid chromatography

Table 1. The identified compounds in NE extracts by searched chemical reference library of standards from the FOODB and HMDB databases

NE extract									
N°	**RT**	**IP**	**Adduct**	**Description**	**NM**	**DM**	**ME**	**S**	**FS**
1	0.89	–	[M–H, M+FA–H]	Gentiotriose	504.169	549.167	–1.02	56.6	85.8
2	1.69	–	[M+FA–H]	Wyomin	n.d	801.206	–4.62	46.6	48.8
3	3.25	–	[M+FA–H]	1-*O*-Sinapoylglucose	n.d	431.118	–1.74	53.7	71.6
4	4.17	–	[2M–H]	Edulisin VI	n.d	811.245	0.33	44.4	33.3
5	4.57	–	[M+FA–H]	1-Octen-3-yl primeveroside	n.d	467.212	–1.54	53.7	71.6
6	0.79	+	[M+H–H_2O, M+H]	*D*-1-[(3-Carboxypropyl) amino]-1-deoxyfructose	265.116	266.123	–0.14	57.9	86.4
7	0.89	+	[M+NH_4, M+Na]	Umbelliferose	504.170	527.158	0.07	56	83.9
8	1.66	+	[M+H–H_2O, M+H]	4-Hydroxycinnamic acid	164.047	147.044	0.17	53.8	71.4
9	3.22	+	[M+H–H_2O]	2-Hydroxycinnamic acid	n.d	147.044	0.14	47.9	41.9
10	4.16	+	[M+H–H_2O]	Inulobiose	n.d	365.105	–0.52	54.9	79.7

DM: detected mass (m/z); ESI: electrospray ionization; FS: fragmentation score (max 0–100%); FOODB: Food Database; HMDB: Human Metabolome Database; IP: ionization polarize mode (negative and positive ESI); ME: mass error (< 5 ppm); n.d: no data; NE extract: noni ethanol extract; NM: neutral mass (m/z); RT: retention time (t_r = min); S: score (max 30–60%)

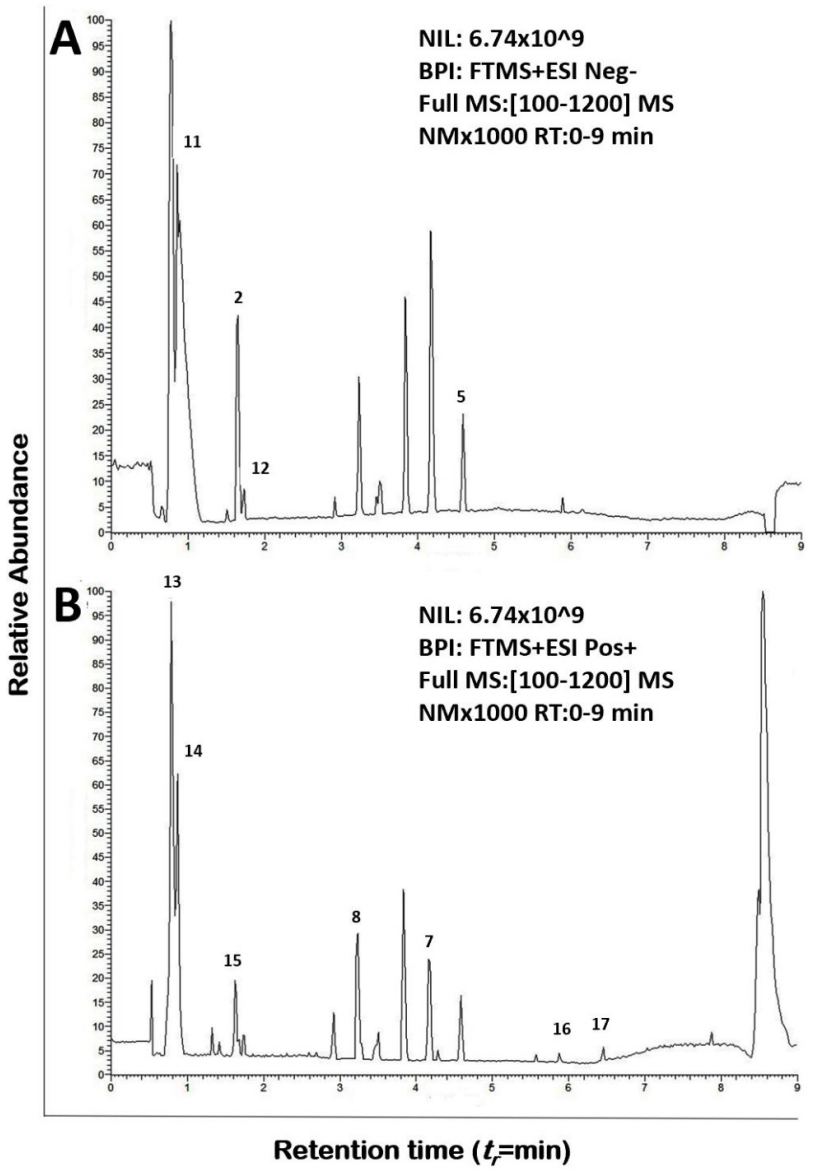

Figure 8. Illustration of the UPLC analysis chromatogram, which displays the peak counts and retention time (*tr* = min) relative to the abundance of both negative (ESI–) and positive (ESI+) ions BPI graphs (NM extract). The chromatograms are divided into two sections: (**A**) showing the peak counts of identified compounds peaks (2, 5, 11, 12) in the NM extract using ESI–, (**B**) displaying the peak counts (7, 8, 13–17) in the NM extract using ESI+. BPI: base peak intensity; ESI: electrospray ionization; NM: noni methanol; UPLC: ultra-performance liquid chromatography

Herein, the identified compounds in NE and NM extract with chemical formular (CF) and molecular weight (MW, g·mol^{-1}) as follows. Peak 1 (t_r = 0.89) Gentiotriose (CF: $C_{18}H_{32}O_{16}$, MW: 504.4371), also known as isomaltotriose, is an oligosaccharide and has been detected in fruits [45]. Peak 2 (t_r = 1.69) Wyomin (CF: $C_{33}H_{40}O_{20}$, MW: 756.6587), belongs to the class of flavonoid-7-*O*-glycosides compounds. It was one of the phenolic compounds that have been detected in several different foods, such as barley (*Hordeum vulgare*), breakfast cereal, cereals, cereal products, common wheat (*Triticum aestivum*), and kinds of wheat (*Triticum*) [45]. Peak 3 (t_r = 3.25) 1-*O*-Sinapoylglucose (CF: $C_{17}H_{22}O_{10}$, MW: 386.3506) belongs to the class of organic compounds known as hydroxycinnamic acid glycosides and has been detected in a few different foods, such as brassicas, Brussel sprouts (*Brassica oleracea* var. gemmifera), and other green vegetables [45]. Peak 4 (t_r = 4.17) Edulisin VI (CF: $C_{20}H_{22}O_9$, MW: 406.3833) belongs to the class of organic compounds known as furanocoumarins, and it has been detected in green vegetables [45]. Peak 5 (t_r = 4.57) 1-Octen-3-yl primeveroside (CF: $C_{19}H_{34}O_{10}$, MW: 422.4673) also seen off NM, was known as fatty acyl glycosides of mono- and disaccharides [45]. Peak 6 (t_r = 0.79) *D*-1-[(3-Carboxypropyl) amino]-1-deoxyfructose (CF: $C_{10}H_{19}NO_7$, MW: 265.2604) is a gamma-amino acid and derivative compound and has been detected in fruits [45]. Peak 7 (t_r = 0.89) Umbelliferose (CF: $C_{18}H_{32}O_{16}$, MW: 504.4371), also identified at (t_r = 4.16) of

NM extract, belongs to the class of organic compounds known as *O*-glycosyl compounds, and it has been detected in several different foods, such as carrots (*Daucus carota* ssp. sativus), fats and oils, green vegetables, herbs, and spices [45]. Peak 8 (t_r = 1.66) 4-Hydroxycinnamic acid (CF: $C_9H_8O_3$, MW: 164.158), also known as *p*-Coumaric acid, which was also seen to appear at (t_r = 3.23) in the NM sample. It was a coumaric corrosive and plays a significant part as a plant metabolite. On average, this compound has been found in the highest concentration in pineapples, sunflowers, and pepper (*Capsicum frutescens*), and in a lower concentration in spinach, kiwis, and sweet oranges [45]. Importantly, this compound was reported to show promising anticarcinogenic potential for the development of new antitumor agents, adhering to the trend of drugs with greater tolerance and biological effectiveness and the synthesis of derivatives with good antiparasitic profiles [46]. Adiposity caused by a high-fat diet, non-alcoholic fatty liver disease, other metabolic disturbances, and acute lung injury are all ameliorated by the compound's anti-inflammatory and antioxidant properties [47]. Peak 9 (t_r = 3.22) 2-Hydroxycinnamic acid (CF: $C_9H_8O_3$, MW: 164.158), also known as *O*-coumaric acid, has been found in a few different foods, such as corns, hard wheats, and olives and in a lower concentration in pomegranates, cranberries, peanuts, carrots, soybeans, ryes, rye bread, and turmeric [45]. Moreover, it was shown to be an antioxidant [48] and a potential among phenolic acids used as effective in the inhibition of antibiotic-resistant pathogenic bacteria [49]. Peak 10 (t_r = 4.16) Inulobiose (CF: $C_{12}H_{22}O_{11}$, MW: 342.2965), also known as difructan or inulin, belongs to the class of *C*-glycosyl compounds.

NM extract, as seen in Figure 8A (top ESI–), and Figure 8B (bottom ESI+), are both the BPI graph, which showed 11 identified compound peaks, of which 4 were identical and were present in NE analyzed extracts. The 7 remaining unique compounds present in the NM extracts were listed and categorized accordingly in Table 2. Peak 11 (t_r = 0.86) Sakebiose (CF: $C_{12}H_{22}O_{11}$, MW: 342.2965), also known as nigerose, belongs to *O*-glycosyl compounds. It has been detected in fruits [45]. Peak 12 (t_r = 1.73) Riboflavin (CF: $C_{17}H_{20}N_4O_6$, MW: 376.3639) or vitamin B2 is an easily absorbed, water-soluble micronutrient with a key role in maintaining human health [50]. The disparate findings of numerous studies attempting to link B vitamins to the development of cancer are clarified by previous studies, which demonstrated that riboflavin plays an evident role in immune cell regulation [51]. Interestingly, a recent report mentioned that riboflavin is a safer option for critically ill COVID-19 patients, especially those in high-risk categories, established as an alternative [52]. It was known as an antioxidant and anti-inflammasome that regulates the inflammatory response [53]. Riboflavin deficiency offered new insights into the role in esophageal carcinogenesis [54]. Peak 13 (t_r = 0.78) *N*-(1-Deoxy-1-fructosyl) alanine (CF: $C_9H_{17}NO_7$, MW: 251.2338) is a class of organic compounds known as *C*-glycosyl compounds, and it is detected in green vegetables and root vegetables [45]. Peak 14 (t_r = 0.87) is β-*D*-Galactopyranosyl-(1->3)-β-*D*-galactopyranosyl-(1->6)-*D*-galactose (CF: $C_{18}H_{32}O_{16}$, MW: 504.4371), which is known as an oligosaccharide and has been detected in fruits [45]. Peak 15 (t_r = 1.62) 1-Oxo-1*H*-2-benzopyran-3-carboxaldehyde (CF: $C_{10}H_6O_3$, MW: 174.1528), also known as 3-formylisocoumarin or artemidinal, belongs to the class of iso-coumarins and derivatives [45]. Peak 16 (t_r = 5.88) 1-(β-*D*-Glucopyranosyloxy)-3-octanone (CF: $C_{18}H_{32}O_{16}$, MW: 504.4371) is a fatty acyl glycoside of mono- and disaccharides [45]. Peak 17 (t_r = 6.46) Armillaripin (CF: $C_{24}H_{30}O_6$, MW: 414.4914) belongs to the class of organic compounds and is known as melleolides and analogues of lipids [45].

Table 2. The identified compounds in NM extracts by searched chemical reference library of standards from the FOODB and HMDB databases

NM extract									
N°	RT	IP	Adduct	Description	NM	DM	ME	S	FS
2	1.65	–	[M+FA–H]	Wyomin	n.d	801.2062	–4.30	47.3	51.5
5	4.59	–	[M+FA–H]	1-Octen-3-yl primeveroside	n.d	467.2127	–1.61	55.4	80.9
7	4.16	+	[M+H–H_2O]	Umbelliferose	n.d	487.1658	0.08	55.3	81.9
8	3.23	+	[M+H–H_2O, M+H]	4-Hydroxycinnamic acid	164.047	147.0441	–0.24	56.8	86.1
11	0.86	–	[M+FA–H, M–H]	Sakebiose	342.116	387.1138	–1.65	56.1	83.7
12	1.73	–	[M+FA–H]	Riboflavin	n.d	421.1349	–4.22	50.7	60.2

Table 2. The identified compounds in NM extracts by searched chemical reference library of standards from the FOODB and HMDB databases (*continued*)

NM extract									
N°	**RT**	**IP**	**Adduct**	**Description**	**NM**	**DM**	**ME**	**S**	**FS**
13	0.78	+	[M+H–H_2O, M+H, M+Na]	*N*-(1-Deoxy-1-fructosyl) alanine	251.104	234.0971	–0.47	58.8	86.5
14	0.87	+	[M+NH_4, M+K, M+Na]	β-*D*-Galactopyranosyl-(1->3)-β-*D*-galactopyranosyl-(1->6)-*D*-galactose	504.170	527.1582	–0.06	55.7	81.1
15	1.62	+	[M+H]	1-Oxo-1*H*-2-benzopyran-3-carboxaldehyde	n.d	175.0389	–0.20	51.8	60.4
16	5.88	+	[M+H–H_2O]	1-(β-*D*-Glucopyranosyloxy)-3-octanone	n.d	289.1643	–0.77	53.8	72.6
17	6.46	+	[M+H, M+Na, M+NH_4]	Armillaripin	414.204	437.1933	–0.57	41.1	10.8

DM: detected mass (m/z); ESI: electrospray ionization; FS: fragmentation score (max 0–100%); FOODB: Food Database; HMDB: Human Metabolome Database; IP: ionization polarize mode (negative and positive ESI); ME: mass error (< 5 ppm); n.d: no data; NM extract: noni methanol extract; NM: neutral mass (m/z); RT: retention time (t_r = min); S: score (max 30–60%)

Using UPLC-Q-exactive orbitrap-MS/MS, we identified a total of 17 compounds from the alcoholic extracts of Hainan dry noni fruit. They are, respectively, coumarins, flavonoids, phenolic, oligosaccharides, flavonoids of both glycosides' substrates, namely *O*-glycosyl and *C*-glycosyl, coumaric acids, phenol lipids, melleolides, and fatty acyl glycoside compounds [44, 45]. To confirm their individual molecular structures and other physical and chemical properties from the HMDB and FOODB databases, the compounds were cross-referenced to the National Institute of Standards and Technology (NIST) and Open Chemistry database-National Library of Medicine-National Center of Biotechnology Information (PubChem-NCBI) of the identifiers. Herein, the identified compounds in NE and NM extract are presented with their molecular structures: compounds (1) to (7) in Figure 9, compounds (8) to (17) in Figure 10. Among the 17 compounds, other 14 phytocompounds were identified from noni fruit for the first time, except 4-Hydroxycinnamic acid (peak 8), 2-Hydroxycinnamic acid (peak 9), and Riboflavin (peak 12).

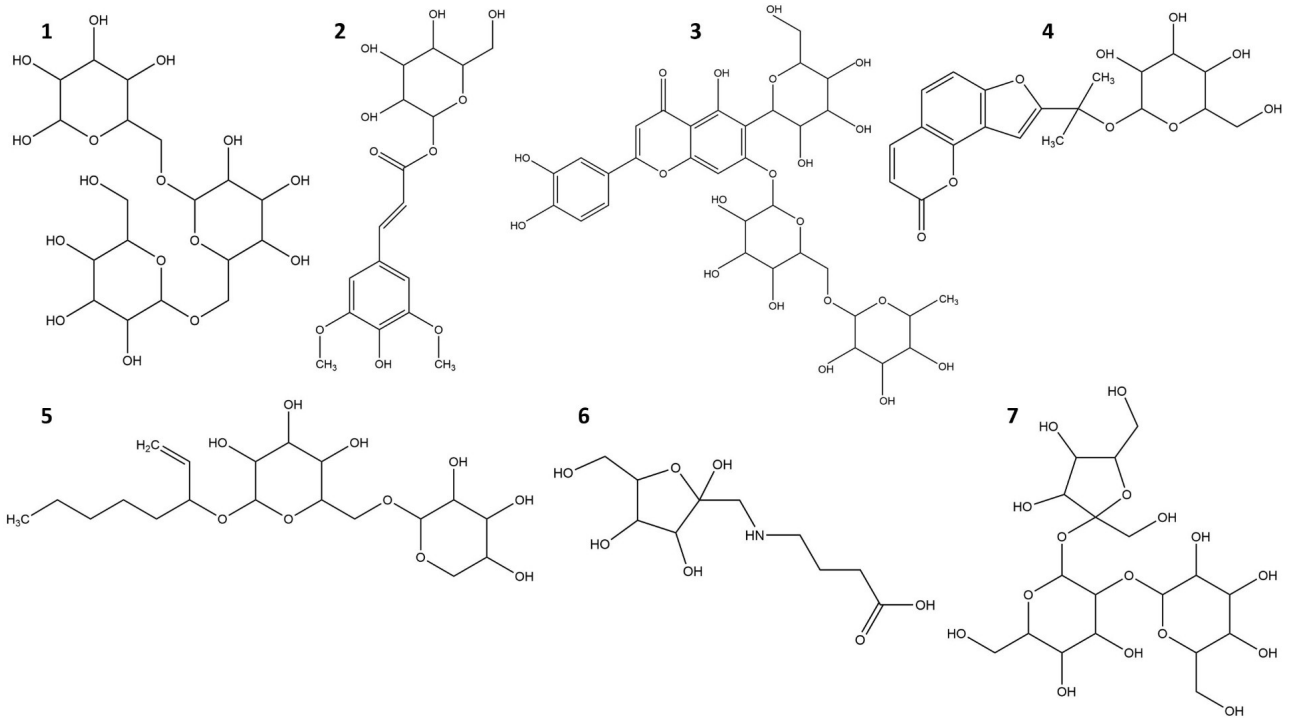

Figure 9. Illustrates the molecular structures of the identified phytoconstituents corresponding to peak count 1 to 7. (1) Gentiotriose, (2) Wyomin, (3) 1-*O*-Sinapoylglucose, (4) Edulisin VI, (5) 1-Octen-3-yl primeveroside, (6) *D*-1-[(3-Carboxypropyl) amino]-1-deoxyfructose, and (7) Umbelliferose

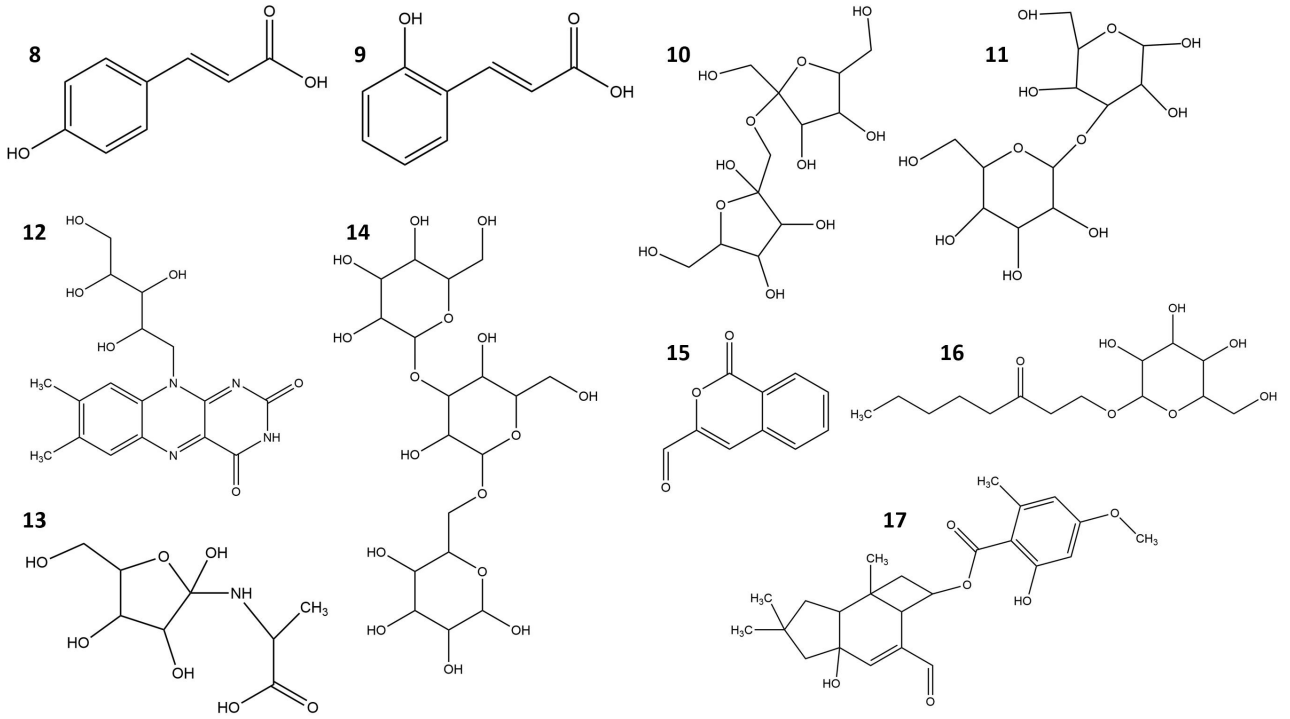

Figure 10. Illustrates the molecular structures of identified phytoconstituents corresponding to peak counts 8 to 17. (8) 4-Hydroxycinnamic acid, (9) 2-Hydroxycinnamic acid, (10) Inulobiose, (11) Sakebiose, (12) Riboflavin, (13) *N*-(1-Deoxy-1-fructosyl) alanine, (14) β-*D*-Galactopyranosyl-(1->3)-β-*D*-galactopyranosyl-(1->6)-*D*-galactose, (15) 1-Oxo-1*H*-2-benzopyran-3-carboxaldehyde, (16) 1-(β-*D*-Glucopyranosyloxy)-3-octanone, and (17) Armillaripin

Discussion

The efficacy of hydroalcoholic solvent extraction aided by modern extraction techniques is a viable method for recovering valuable compounds from noni fruit. Studies have consistently highlighted the antibacterial, anticancer, and other therapeutic properties of noni, emphasizing the need for further investigation into its fruit [4, 9, 20]. Previous research has corroborated the efficacy of these methods in extracting valuable compounds from diverse noni plant materials, including leaves and bark [2, 5–8]. For instance, studies on the extraction of bioactive compounds from noni fruit, leaves, and bark using different solvents have revealed significant variations in extraction efficiency. The findings suggest that the choice of solvents and extraction technique does play a crucial role in determining the yield and quality of extracted compounds [8, 9, 13–17]. Our study demonstrated that the use of hydro-alcohol solvents, such as EtOH and MeOH, in combination with advanced extraction techniques, including the KBE-I5 extractor, followed by vacuum drying, effectively yielded extracts of NE and NM with high recovery rates.

The noni plant has been extensively studied for its various medicinal properties, and its extracts have been found to exhibit antimicrobial effects and therapeutic benefits for health-related issues [1–19]. In our study, the NE and NM extracts demonstrated positive antimicrobial and anticancer effects on several harmful microbial strains and cancer cell lines, as reported. Specifically, both hydroalcoholic fruit extracts exhibited positive inhibitory effects on bacterial strains, including EC, SA, ST, and the fungal strain SC, with the measured inhibition zones and evaluated MIC values. Both noni extracts demonstrated a selective cytotoxic effect, inhibiting the growth of HT-29 and UMUC-3 while sparing non-cancerous cells HUVEC and SVHUC-1. The noni extracts decreased cell viability, and microscopic examination revealed irregularly shaped organelles in treated cells, indicative of cellular damage. The observed morphological changes were attributed to the inhibitory effects of the extracts at their respective IC_{50}s after a 72 h exposure. In contrast, the control group exhibited normal cellular morphology, highlighting the specificity of the extracts' cytotoxic effects towards cancerous cells. Using AO as a fluorescent stain, a method widely utilized for visualizing acidic organelles such as autophagosomes [38, 39], thus in this study we show evidence supporting the efficacy of NE and NM extracts against HT-29 and UMUC-3 cells. This was demonstrated through the induction and accumulation of autophagic vesicles within these cells, which were detectable via

fluorescence emission. The western blot analysis demonstrated increased expression levels of the LC3A II/I protein in HT-29 and UMUC-3 cells, indicating that autophagy was the mechanism leading to cell death after treatment with NE and NM extracts.

Most importantly, the fruit has been shown to contain several phytoconstituents exhibiting therapeutic importance for various health benefits [10–21]. Therefore, the accurate identification of these phytoconstituents is highly dependent on the efficiency of the extraction process, which critically influences their subsequent effective detection using advanced analytical techniques [8, 9, 12–14]. Using UPLC-Q-exactive orbitrap-MS/MS analysis and the application of a chemical reference library of standards databases, a total of 17 compounds were identified in the NE and NM extracts. This analytical approach is widely recognized for its efficacy in the comprehensive profiling of complex natural product matrices of noni fruit [13, 18, 19]. Among these identified compounds, riboflavin, 4-Hydroxycinnamic acid, and 2-Hydroxycinnamic acid are notable, having been previously recognized and investigated for their health-related properties, leaving the remaining 14 novel phytoconstituents identified in (*Morinda citrifolia* L.) noni fruit extracts.

In conclusion, NE and NM exhibited significant antimicrobial and anticancer properties. Hence, the noni fruit could serve as an alternative to antimicrobial and anticancer agents when consumed for nutritional purposes or utilized therapeutically owing to its pharmaceutical properties. Furthermore, isolating these novel phytoconstituents in this study contributes to the existing knowledge on noni fruit composition and paves the way for future bioactive studies exploring their nutritional and therapeutic properties.

Abbreviations

AO: acridine orange

Arb: arbitrary

BPI: base peak intensity

CCK-8: cell counting kit-8

CCS: collisional cross section

CF: chemical formular

CO_2: carbon dioxide

DMEM: Dulbecco's modified Eagle's medium

DMSO: dimethyl sulfoxide

EC: *Escherichia coli*

ESI: electrospray ionization

EtOH: ethanol

FOODB: Food Database

GC-MS: gas chromatography-mass spectrometry

HCID: high collision-induced dissociation

HMDB: Human Metabolome Database

HT-29: human colon adenocarcinoma cell

HUVEC: human umbilical vein endothelial cell

IC_{50}: half inhibitory concentration

LB: Luria-Bertani

LCID: low collision-induced dissociation

MeOH: methanol

MIC: minimum inhibitory concentration

MW: molecular weight

NaCl: sodium chloride

NE: noni ethanol

NM: noni methanol

PBS: phosphate-buffered saline

RT: retention time

SA: *Staphylococcus aureus*

SC: *Saccharomyces cerevisiae*

SDS: sodium dodecyl sulfate

SMPDB: Small Molecule Pathway Database

ST: *Streptococcus thermophilus*

SVHUC-1: human uroepithelium bladder cell line

T3DB: Toxin and Toxin Target Database

UMUC-3: human bladder cancer cell

UPLC-Q-exactive orbitrap-MS/MS: ultra-performance liquid chromatography quadrupole exactive orbitrap-tandem mass spectrometer

YPD: yeast peptone dextrose

Declarations

Acknowledgments

As the author, I, Dr Aslee Tailulu, would like to express my sincere gratitude toward Mr. Feng Sijia from the Shanghai OE Biotech. Co., Ltd., based in Shanghai, China, for his invaluable assistance in providing analysis assistance and database access. This support was crucial to the successful completion of my research. I am also deeply grateful to my wife, Mrs. Brenna Marie McFadden, and my daughter, Ms. Elizabeth Dode Tailulu, for their unwavering support, their patience, and their constant encouragement throughout the duration of this long and exciting research project and article writing period. Their presence and understanding were instrumental in seeing this project through to its completion.

Author contributions

AT: Conceptualizing, Methodology, Validation, Formal analysis, Investigation, Resources, Data curation, Software, Visualization, Project administration, Writing—original draft, Writing—review & editing. HC: Methodology, Formal analysis, Data curation. LW: Methodology, Formal analysis, Data curation, Writing—review & editing. YS: Funding acquisition. PS: Conceptualization, Formal analysis, Writing—review & editing, Funding acquisition, Supervision. All authors agree to be accountable for all aspects of work, ensuring integrity and accuracy.

Conflicts of interest

The authors declare that they have no known competing financial interests or personal relationships that could have appeared to influence the work reported in this paper.

Ethical approval

Not applicable.

Consent to participate

Not applicable.

Consent to publication

Not applicable.

Availability of data and materials

All data were generated in-house, and no paper mill was used. Requests for accessing the datasets should be directed to Aslee Tailulu, y10180458@mail.ecust.edu.cn.

Funding

This work was supported by the Key Laboratory Project of Qinghai Science & Technology Department and the Open Project of Laboratory for Research and Utilization of Qinghai Tibet Plateau Germplasm Resources [Grant ID: 2023-SYS-01]; and the National Natural Science Foundation of China [Grant ID: 32171958]. The funders had no role in study design, data collection and analysis, decision to publish, or preparation of the manuscript.

Publisher's note

Open Exploration maintains a neutral stance on jurisdictional claims in published institutional affiliations and maps. All opinions expressed in this article are the personal views of the author(s) and do not represent the stance of the editorial team or the publisher.

References

1. Almeida ÉS, de Oliveira D, Hotza D. Properties and Applications of *Morinda citrifolia* (Noni): A Review. Compr Rev Food Sci Food Saf. 2019;18:883–909. [DOI] [PubMed]
2. Jahurul MHA, Patricia M, Shihabul A, Norazlina MR, Ramlah George MR, Noorakmar AW, et al. A review on functional and nutritional properties of noni fruit seed (*Morinda citrifolia* L.) and its oil. Food Biosci. 2021;41:101000. [DOI]
3. Mahomoodally MF, Mootoosamy A, Wambugu S. Traditional Therapies Used to Manage Diabetes and Related Complications in Mauritius: A Comparative Ethnoreligious Study. Evid Based Complement Alternat Med. 2016;2016:4523828. [DOI] [PubMed] [PMC]
4. Zhang C, Quek SY, Fu N, Su Y, Kilmartin PA, Chen XD. Storage stability and *in vitro* digestion of microencapsulated powder containing fermented noni juice and probiotics. Food Biosci. 2020;37:100740. [DOI]
5. Torres MAO, de Fátima Braga Magalhães I, Mondêgo-Oliveira R, de Sá JC, Rocha AL, Abreu-Silva AL. One Plant, Many Uses: A Review of the Pharmacological Applications of *Morinda citrifolia*. Phytother Res. 2017;31:971–9. [DOI] [PubMed]
6. Singh B, Sharma RA. Indian Morinda species: A review. Phytother Res. 2020;34:924–1007. [DOI] [PubMed]
7. Ahmad AN, Mat Daud ZA, Ismail A. Review on potential therapeutic effect of *Morinda citrifolia* L. Curr Opin Food Sci. 2016;8:62–7. [DOI]
8. Li J, Niu D, Zhang Y, Zeng X. Physicochemical properties, antioxidant and antiproliferative activities of polysaccharides from *Morinda citrifolia* L. (Noni) based on different extraction methods. Int J Biol Macromol. 2020;150:114–21. [DOI] [PubMed]
9. Zhang B, Zhou X, Zhao T, Wang J, Li M, Lyu S, et al. Chemical constituents from fermented Noni juice. Zhongguo Zhong Yao Za Zhi. 2019;44:4015–20. Chinese. [DOI] [PubMed]

10. Oh JS, Seong GS, Kim YD, Choung SY. Effects of Deacetylasperulosidic Acid on Atopic Dermatitis through Modulating Immune Balance and Skin Barrier Function in HaCaT, HMC-1, and EOL-1 Cells. Molecules. 2021;26:3298. [DOI] [PubMed] [PMC]
11. Kim SH, Seong GS, Choung SY. Fermented *Morinda citrifolia* (Noni) Alleviates DNCB-Induced Atopic Dermatitis in NC/Nga Mice through Modulating Immune Balance and Skin Barrier Function. Nutrients. 2020;12:249. [DOI] [PubMed] [PMC]
12. Lohani M, Majrashi M, Govindarajulu M, Patel M, Ramesh S, Bhattacharya D, et al. Immunomodulatory actions of a Polynesian herb Noni (*Morinda citrifolia*) and its clinical applications. Complement Ther Med. 2019;47:102206. [DOI] [PubMed]
13. Tasfiyati AN, Antika LD, Dewi RT, Septama AW, Sabarudin A, Ernawati T. An experimental design approach for the optimization of scopoletin extraction from *Morinda citrifolia* L. using accelerated solvent extraction. Talanta. 2022;238:123010. [DOI] [PubMed]
14. Narasingam M, Vijeepallam K, Mohamed Z, Pandy V. Anxiolytic- and antidepressant-like activities of a methanolic extract of *Morinda citrifolia* Linn. (noni) fruit in mice: Involvement of benzodiazepine-$GABA_A$ergic, serotonergic and adrenergic systems. Biomed Pharmacother. 2017;96: 944–52. [DOI] [PubMed]
15. Zhu H, Zhang J, Li C, Liu S, Wang L. *Morinda citrifolia* L. leaves extracts obtained by traditional and eco-friendly extraction solvents: Relation between phenolic compositions and biological properties by multivariate analysis. Ind Crops Prod. 2020;153:112586. [DOI]
16. Deng S, West BJ, Palu AK, Jensen CJ. Determination and comparative analysis of major iridoids in different parts and cultivation sources of *Morinda citrifolia*. Phytochem Anal. 2011;22:26–30. [DOI] [PubMed]
17. Qin D, Xi J. Flash extraction: An ultra-rapid technique for acquiring bioactive compounds from plant materials. Trends Food Sci Technol. 2021;112:581–91. [DOI]
18. Tailulu A, Li M, Ye B, Al-Qudaimi R, Cao F, Liu W, et al. Antimicrobial and anticancer activities of Hainan dry noni fruit alcoholic extracts and their novel compounds identification using UPLC-Q-Exactive Obitrap-MS/MS. J Pharm Biomed Anal. 2022;220:114989. [DOI] [PubMed]
19. TaiLulu A, Li M, Zheng Q, Zhu Z, Wang H, Jiang Q, et al. Identification of antimicrobial active components from dry Hainan *Morinda citrifolia* linn (Noni) fruit using GC-MS. Int J Food Sci Nutr. 2021;6:65–71.
20. Deng S, West BJ, Jensen CJ. A quantitative comparison of phytochemical components in global noni fruits and their commercial products. Food Chem. 2010;122:267–70. [DOI]
21. Al-qudaimi R, Zheng Q, Tailulu A, Zhu Z, Shi P. A Capillary Zone Electrophoresis Method for Selenite Detection in Culture Media for Total Selenium Determination in Yeast Cells. J Anal Chem. 2023;78: 247–55. [DOI]
22. Zhu P, Wang S, Wang J, Zhou L, Shi P. A capillary zone electrophoresis method for adenine nucleotides analysis in *Saccharomyces cerevisiae*. J Chromatogr B Analyt Technol Biomed Life Sci. 2016;1008: 156–63. [DOI] [PubMed]
23. Zhu P, Wang S, Wang J, Zhou L, Shi P. Simultaneous analysis of adenosine triphosphate and its metabolites in *Saccharomyces cerevisiae* using RP-HPLC. Acta Chromatogr. 2016;28:501–11. [DOI]
24. Wang J, Wang S, Yan C, Deng Y, Huang Z, Shi P. Mass spectrometry-based proteomic analysis reveals the interacting partners of lipin1. IUBMB Life. 2018;70:753–62. [DOI] [PubMed]
25. Zhang L, Liu S, Chen Y, Guo J, Li C, Zhang J. Metatranscriptomic approach reveals the functional and enzyme dynamics of core microbes during noni fruit fermentation. Food Res Int. 2021;141:109999. [DOI] [PubMed]
26. Zhu P, Li M, Yan C, Sun J, Peng M, Huang Z, et al. Aspirin Causes Lipid Accumulation and Damage to Cell Membrane by Regulating *DCI1*/ *OLE1* in *Saccharomyces cerevisiae*. Microb Drug Resist. 2020;26: 857–68. [DOI] [PubMed]

27. Li M, Zhu P, Huang Z, Huang Y, Lv X, Zheng Q, et al. Aspirin damages the cell wall of *Saccharomyces cerevisiae* by inhibiting the expression and activity of dolichol-phosphate mannose synthase 1. FEBS Lett. 2022;596:369–80. [DOI] [PubMed]
28. Li B, Zhen H, Zhang X, Wang S, Zhang Y, Fang Z, et al. Probiotic properties of *Enterococcus* strains isolated from the silage. J Food Saf. 2015;35:108–18. [DOI]
29. Wang J, Li B, Zhou L, Zhang X, Shi P. Probiotic potential and function of a *Lactobacillus* strain L1 isolated from Silage. J Food Saf. 2017;37:e12338. [DOI]
30. Li M, Sun P, Dong K, Xin Y, TaiLulu A, Li Q, et al. Chemerin reverses the malignant phenotype and induces differentiation of human hepatoma SMMC7721 cells. Arch Pharm Res. 2021;44:194–204. [DOI] [PubMed]
31. Doğan Y, Öziç C, Ertaş E, Baran A, Rosic G, Selakovic D, et al. Activated carbon-coated iron oxide magnetic nanocomposite (IONPs@CtAC) loaded with morin hydrate for drug-delivery applications. Front Chem. 2024;12:1477724. [DOI] [PubMed] [PMC]
32. Öziç C, Ertaş E, Baran MF, Baran A, Ahmadian E, Eftekhari A, et al. Synthesis and characterization of activated carbon-supported magnetic nanocomposite (MNPs-OLAC) obtained from okra leaves as a nanocarrier for targeted delivery of morin hydrate. Front Pharmacol. 2024;15:1482130. [DOI] [PubMed] [PMC]
33. Li M, Xia S, Shi P. DPM1 expression as a potential prognostic tumor marker in hepatocellular carcinoma. PeerJ. 2020;8:e10307. [DOI] [PubMed] [PMC]
34. Xu Z, Ye B, Li M, Fan Z, Sun J, Huang Z, et al. The expression of SLFN11 is related to the sensitivity of bladder cancer cells to DNA damage agents. Gene Rep. 2024;34:101881. [DOI]
35. Cui H, Xin Y, Cao F, Gan Z, Tian Y, Liu W, et al. The correlation between CpG island methylation of hTERT promoter and human age prediction. Leg Med. 2023;63:102270. [DOI] [PubMed]
36. Wang J, Wang S, Zhang X, Hu L, Shi P. Artemisinin Reduces Lipid Accumulation in Hepatocytes by Inhibition of CD36 Expression. Indian J Pharm Educ Res. 2017;51:393–400. [DOI]
37. Matuschek E, Brown DFJ, Kahlmeter G. Development of the EUCAST disk diffusion antimicrobial susceptibility testing method and its implementation in routine microbiology laboratories. Clin Microbiol Infect. 2014;20:O255–66. [DOI] [PubMed]
38. Ertaş E, Doğan S, Baran A, Baran MF, Evcil M, Kurt B, et al. Preparation and Characterization of Silver-Loaded Magnetic Activated Carbon Produced from *Crataegus Monogyna* for Antimicrobial and Antioxidant Applications. Chemistry Select. 2025;10:e202405558. [DOI]
39. Baran A, Ertaş E, Baran MF, Eftekhari A, Gunes Z, Keskin C, et al. Green-Synthesized Characterization, Antioxidant and Antibacterial Applications of CtAC/MNPs-Ag Nanocomposites. Pharmaceuticals (Basel). 2024;17:772. [DOI] [PubMed] [PMC]
40. Lv X, Fan Z, Cao F, Liu W, Huang Z, Shi P. Clioquinol induces autophagy by down-regulation of calreticulin in human neurotypic SH-SY5Y cells. Chem Biol Interact. 2023;369:110268. [DOI] [PubMed]
41. Lv X, Zheng Q, Li M, Huang Z, Peng M, Sun J, et al. Clioquinol induces S-phase cell cycle arrest through the elevation of the calcium level in human neurotypic SH-SY5Y cells. Metallomics. 2020;12:173–82. [DOI] [PubMed]
42. Shi P, Lai R, Lin Q, Iqbal AS, Young LC, Kwak LW, et al. IGF-IR tyrosine kinase interacts with NPM-ALK oncogene to induce survival of T-cell ALK+ anaplastic large-cell lymphoma cells. Blood. 2009;114: 360–70. [DOI] [PubMed] [PMC]
43. TaiLulu A, Shi P. A study on protein extraction of noni dry and fresh fruit with polyacrylamide gel electrophoresis. Int J Food Sci Nutr. 2022;7:10–7.
44. Wishart DS, Guo AC, Oler E, Wang F, Anjum A, Peters H, et al. HMDB 5.0: The Human Metabolome Database for 2022. Nucleic Acids Res. 2022;50:D622–31. [DOI] [PubMed] [PMC]
45. Yannai S, editor. Dictionary of Food Compounds with CD-ROM. 2nd ed. Boca Raton: CRC Press; 2012.

46. Gastaldello GH, Cazeloto ACV, Ferreira JC, Rodrigues DM, Bastos JK, Campo VL, et al. Green Propolis Compounds (Baccarin and p-Coumaric Acid) Show Beneficial Effects in Mice for Melanoma Induced by B16f10. Medicines (Basel). 2021;8:20. [DOI] [PubMed] [PMC]
47. Yoon DS, Cho SY, Yoon HJ, Kim SR, Jung UJ. Protective effects of p-coumaric acid against high-fat diet-induced metabolic dysregulation in mice. Biomed Pharmacother. 2021;142:111969. [DOI] [PubMed]
48. Sharma P, Singh R. Efficacy of trans-2-hydroxycinnamic Acid against trichlorfon-induced oxidative stress in wistar rats. Toxicol Int. 2012;19:295–300. [DOI] [PubMed] [PMC]
49. Keman D, Soyer F. Antibiotic-Resistant *Staphylococcus aureus* Does Not Develop Resistance to Vanillic Acid and 2-Hydroxycinnamic Acid after Continuous Exposure in Vitro. ACS Omega. 2019;4: 15393–400. [DOI] [PubMed] [PMC]
50. Phan T, Sun L, Bay B, Chan S, Lee S. Dietary compounds inhibit proliferation and contraction of keloid and hypertrophic scar-derived fibroblasts in vitro: therapeutic implication for excessive scarring. J Trauma. 2003;54:1212–24. [DOI] [PubMed]
51. Peterson CT, Rodionov DA, Osterman AL, Peterson SN. B Vitamins and Their Role in Immune Regulation and Cancer. Nutrients. 2020;12:3380. [DOI] [PubMed] [PMC]
52. Ragan I, Hartson L, Pidcoke H, Bowen R, Goodrich R. Pathogen reduction of SARS-CoV-2 virus in plasma and whole blood using riboflavin and UV light. PLoS One. 2020;15:e0233947. [DOI] [PubMed] [PMC]
53. Colasuonno F, Bertini E, Tartaglia M, Compagnucci C, Moreno S. Mitochondrial Abnormalities in Induced Pluripotent Stem Cells-Derived Motor Neurons from Patients with Riboflavin Transporter Deficiency. Antioxidants (Basel). 2020;9:1252. [DOI] [PubMed] [PMC]
54. Jin C, Yonezawa A, Yoshimatsu H, Imai S, Koyanagi M, Yamanishi K, et al. Effect of riboflavin deficiency on development of the cerebral cortex in Slc52a3 knockout mice. Sci Rep. 2020;10:18443. [DOI] [PubMed] [PMC]